JACC: BASIC TO TRANSLATIONAL SCIENCE VOL. 6, NO. 4, 2021

PRECLINICAL RESEARCH

Injectable Myocardial Matrix Hydrogel Mitigates Negative Left Ventricular Remodeling in a Chronic Myocardial Infarction Model

Miranda D. Diaz, BS,[a,b] Elaine Tran,[a,b] Martin Spang, PhD,[a,b] Raymond Wang, PhD,[a,b] Roberto Gaetani, PhD,[a,b,c] Colin G. Luo, MS,[a,b] Rebecca Braden, MS,[a,b] Ryan C. Hill, PhD,[e] Kirk C. Hansen, PhD,[e] Anthony N. DeMaria, MD,[d] Karen L. Christman, PhD[a,b]

VISUAL ABSTRACT

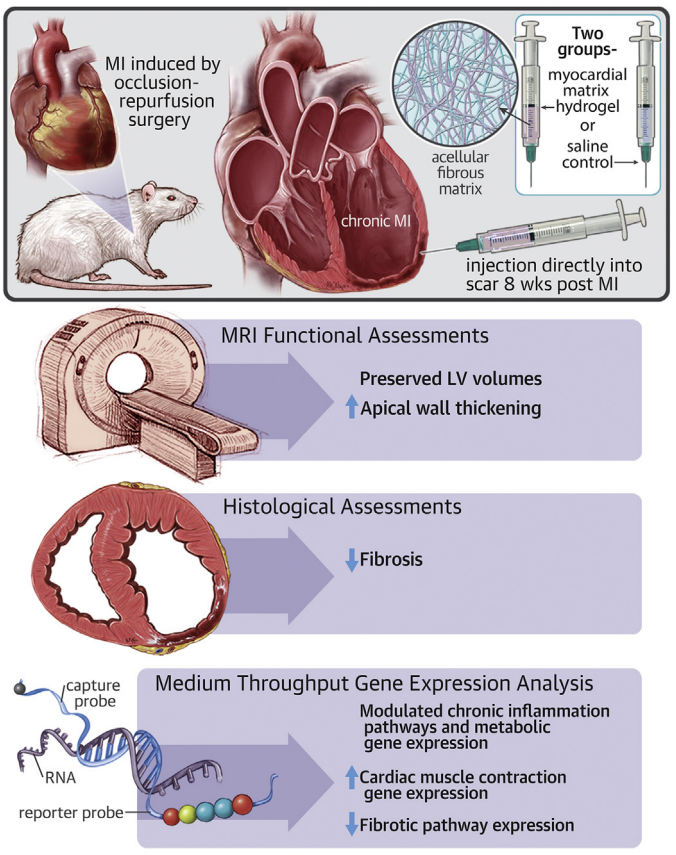

Diaz, M.D. et al. J Am Coll Cardiol Basic Trans Science. 2021;6(4):350–61.

HIGHLIGHTS

- **Myocardial matrix hydrogel preserves LV volumes and apical wall thickening in a chronic MI model.**
- **Myocardial matrix hydrogel trends toward reduced fibrosis.**
- **In vivo differential gene expression analysis shows the matrix modulates cardiac muscle contraction, metabolism, fibrosis, and the inflammatory/immune response in a chronic MI model.**

From the [a]Department of Bioengineering, University of California, San Diego, La Jolla, California, USA; [b]Sanford Consortium for Regenerative Medicine, La Jolla, California, USA; [c]Department of Molecular Medicine, Sapienza University of Rome, Rome, Italy; [d]Department of Medicine, University of California, San Diego, La Jolla, California, USA; and the [e]Department of Biochemistry and Molecular Genetics, Anschutz Medical Campus, University of Colorado, Aurora, Colorado, USA.

ISSN 2452-302X https://doi.org/10.1016/j.jacbts.2021.01.003

SUMMARY

A first-in-man clinical study on a myocardial-derived decellularized extracellular matrix hydrogel suggested the potential for efficacy in chronic myocardial infarction (MI) patients. However, little is understood about the mechanism of action in chronic MI. In this study, the authors investigated the efficacy and mechanism by which the myocardial matrix hydrogel can mitigate negative left ventricular (LV) remodeling in a rat chronic MI model. Assessment of cardiac function via magnetic resonance imaging demonstrated preservation of LV volumes and apical wall thickening. Differential gene expression analyses showed the matrix is able to prevent further negative LV remodeling in the chronic MI model through modulation of the immune response, down-regulation of pathways involved in heart failure progression and fibrosis, and up-regulation of genes important for cardiac muscle contraction. (J Am Coll Cardiol Basic Trans Science 2021;6:350–61)

ABBREVIATIONS AND ACRONYMS

CMR = cardiac magnetic resonance
ECM = extracellular matrix
EDV = end-diastolic volume
EF = ejection fraction
ESV = end-systolic volume
HF = heart failure
IHC = immunohistochemistry
KEGG = Kyoto Encyclopedia of Genes and Genomes
LV = left ventricular
MI = myocardial infarction
MS = mass spectrometry
QconCAT = quantitative concatamer

More than 6 million Americans are currently living with heart failure (HF), and this number is continuing to rise as the average global age increases and therapy of causative conditions improves (1). Currently, there are various injectable biomaterials being investigated for the treatment of myocardial infarction (MI). Although there have been some studies that evaluate these therapeutics in a chronic MI model where the scar has fully formed, the majority of studies have focused on acute or subacute MI models, whereby the material is injected immediately or a short time frame following MI before full scar formation, respectively (2–5). We previously developed a decellularized injectable extracellular matrix (ECM) hydrogel derived from porcine left ventricular (LV) myocardial tissue as a tissue engineering approach for treatment after MI (6). Although the macrostructure of the ECM is broken down in processing, the myocardial matrix hydrogel retains the nanostructure, peptides, and sulfated glycosaminoglycans found in native myocardium and can be delivered minimally invasively via transendocardial delivery. Subacute delivery of the hydrogel 1 to 2 weeks post-MI was previously shown to mitigate negative LV remodeling and improve cardiac function in small and large animal models (6–8). In a rat model of subacute MI, involvement of specific prorepair pathways was found in response to delivery of the hydrogel, including modulation of the inflammatory response, altered metabolism, up-regulation of genes involved in neovascularization, and down-regulation of genes involved in hypertrophy, fibrosis, and apoptosis (8). A first-in-man phase I clinical trial showed initial safety with the decellularized ECM hydrogel therapeutic (9). Although the study was not designed or powered to evaluate efficacy, cardiac magnetic resonance imaging (CMR) analysis suggested that the material may be effective in patients more than 1 year post-MI; however, little is understood about the mechanism of action of the hydrogel in the setting of chronic MI. Therefore, in this study, we aimed to investigate the efficacy and mechanism of action of the myocardial matrix hydrogel in preventing the progression of negative LV remodeling and dysfunction. Understanding the differences in mechanism of action of the material between the subacute and chronic post-MI environments could guide the next phases of clinical testing of the hydrogel, as well as influence the understanding of therapeutic targets for the design of future MI therapeutics.

METHODS

MYOCARDIAL MATRIX PREPARATION AND CHARACTERIZATION. Myocardial matrix was prepared from porcine LV myocardial tissue and characterized as previously outlined (6,10). Briefly, the tissue was chopped, decellularized in sodium dodecyl sulfate detergent, lyophilized, milled into a fine powder, partially enzymatically digested with pepsin in HCl, adjusted for pH and salts, brought to a final concentration of 6 mg/ml, and finally aliquoted and lyophilized for storage at −80°C. When preparing for injection, lyophilized aliquots were resuspended in sterile water approximately 30 min before.

The authors attest they are in compliance with human studies committees and animal welfare regulations of the authors' institutions and Food and Drug Administration guidelines, including patient consent where appropriate. For more information, visit the Author Center.

Manuscript received August 3, 2020; revised manuscript received January 4, 2021, accepted January 4, 2021.

In addition to our standard published assays for quality control, we also performed ECM-targeted, quantitative concatamers (QconCAT) proteomics on the decellularized ECM as previously described (10–12).

SURGICAL PROCEDURES. All procedures in this study were performed in accordance with the guidelines established by the Committee on Animal Research at the University of California, San Diego, and the Association for the Assessment and Accreditation of Laboratory Animal Care. All animals used in the study were adult female Sprague Dawley rats (225 to 250 g). To induce MI, all 48 animals underwent occlusion–reperfusion surgery to occlude the left main artery for 35 min as previously described (6). At 8 weeks post-MI, animals were arbitrarily assigned to injection of 75 ml of either matrix or saline directly into the infarct via subxiphoid access as previously described (6,13).

CMR IMAGING. Cine CMR images were acquired using an 11.7-T Bruker Magnetic Resonance Imaging System by Molecular Imaging (Bruker, Billerica, Massachusetts) at the Sanford Consortium for Regenerative Medicine. Rats were anesthetized using isoflurane in oxygen during imaging. Respiratory and electrocardiogram-gated cine sequences were acquired over contiguous heart axial slices. The following parameters were used: repetition time = 20 ms, echo time = 1.18 ms, flip angle = 30°, field of view = 40 mm^2, data matrix size = 200 × 200. Eight or 9 1.5-mm axial image slices were acquired with a total of 15 cine frames per image slice. ImageJ software, Java 1.8.0_172 (64-bit) (NIH, Bethesda, Maryland) was used to outline the endocardial surface at end-diastole and end-systole for each slice, defined as the minimum and maximum LV lumen area, respectively. Simpson's method was used to calculate the end-diastolic volume (EDV) and end-systolic volume (ESV). Ejection fraction (EF) was calculated as [(EDV − ESV)/EDV] × 100. The myocardium was defined as the area between the epicardium and endocardium. Myocardial area was analyzed at end-diastole and end-systole to assess wall thickening by myocardial area (14,15). Cardiac wall thickening was calculated as [To be consistent with above comment this can be changed to end-diastolic and end-systolic myocardial area (end-diastole myocardial area − end-diastole myocardial area)/end-diastole myocardial area] from cross-sectional MR images the of basal, mid, and apical slices. Rats underwent baseline CMR 2 days before injection of matrix or saline (8 weeks post-MI). Animals that did not have an EF at least 1 SD below healthy values (<68%) were excluded from the study. A total of 24 long-term functional analysis rats underwent the MI procedure; 5 died as a result of the MI, and 5 were excluded on the basis of EF criteria, leaving n = 8 for saline and n = 6 for matrix for final analysis. At 12 weeks post-MI (4 weeks post-injection), rats were imaged, and their cardiac function assessed again for post-treatment evaluation. For wall thickening analysis, 4 animals were excluded due to poor visibility of the myocardium. All CMR acquisition and analyses were performed by investigators blinded to the treatment groups.

TISSUE PROCESSING. At 10 ± 3 days (~1.5 weeks) following final CMR acquisition (~5.5 weeks post-injection, ~13.5 weeks post-MI), the functional set of animals were euthanized, and hearts were fresh frozen in Tissue-Tek O.C.T. Compound (Sakura Finetek, Torrance, California). Once frozen, the hearts were cryosectioned into 10-μm sections. Another set of animals (n = 6 each group) were euthanized at 1 week post-injection (9 weeks post-MI), and their hearts were cut into 7 slices using a stainless-steel rat heart slicer matrix (Zivic Instruments, Pittsburgh, Pennsylvania) with 1.0-mm coronal spacing. The infarct region was isolated from even slices of tissue and flash frozen in liquid nitrogen to preserve RNA as previously described (8). The remaining slices were fresh frozen in Tissue-Tek O.C.T. freezing medium for histology.

HISTOLOGY. Slides from ~5.5-week post-injection animals were sectioned starting ~200 μm from the apex with 16 locations taken at 8 slides per location with 150-μm spacing between each location to span the ventricle. These slides were stained with hematoxylin and eosin or Masson's trichrome, mounted with Permount Mounting Medium (Fisher Chemical, Hampton, New Hampshire), and scanned at 20× using an Aperio ScanScope CS2 slide scanner (Leica Biosystems, Nussloch Germany). Hematoxylin and eosin staining was used to identify 5 representative slides for each animal that were evenly spaced to span the infarct in the ventricle. Trichrome-stained slides were used to assess fibrosis at ~5.5 weeks post-injection using 5 evenly spaced representative slides throughout the infarct scanned at 20× magnification using an Aperio ScanScope CS2 slide scanner. Nonnuclear blue staining was measured using the Positive Pixel Count V9 algorithm within ImageScope software, ImageScope v12.0.1.5027 (Aperio) to determine the collagen content as percentage of infarct area. Interstitial fibrosis was measured as collagen content in noninfarcted septal wall regions.

Immunohistochemistry (IHC) was performed at ~5.5 weeks post-injection using antibodies for the

following antigens: α smooth muscle actin (SMA, 1:75, Agilent M0851, Agilent, Santa Clara, California) and laminin (1:100, Abcam ab11575, Abcam, Cambridge, Massachusetts). Primary antibodies were visualized with secondary antibodies Alexa Fluor 488 or 568 (Life Technologies, Carlsbad, California). Fluorescein-labeled Griffonia Simplicifolia Lectin I isolectin B4 (1:75, Vector Laboratories, Burlingame, California) was also used. Nuclei were stained with Hoechst 33342 (Life Technologies). Following IHC, slides were mounted with Fluoromount (Sigma-Aldrich, St. Louis, Missouri) and imaged at 10× on the Ariol DM6000 B microscope (Leica). For myofibroblast density, the infarct region was traced in each tissue section, and αSMA+-only regions were determined to be myofibroblasts. A MATLAB (MathWorks, Natick, Massachusetts) script was used to identify αSMA+/isolectin− regions, and manual corrections were used to ensure no vessels were included in the quantification, as defined by any stained region with a visible lumen. For analysis of cardiomyocyte hypertrophy at ~5.5 weeks post-injection, 5 regions per laminin-stained slide of the remote myocardium where myocardial fibers were running orthogonal to the plane of the section were randomly selected for analysis. Cross sections of individual cardiomyocytes ($n \geq 300$ cells for each heart) were outlined and the area measured by ImageJ software.

Two of the odd slices (see the Tissue Processing section) from hearts harvested 1 week post-injection were sectioned. The apex slice was excluded due to nonvisible infarct regions. Two locations, 150 mm apart, were taken per matrix tissue slice and 2 slides were taken at each location with a total of 4 tissue sections for each stain. IHC was performed using antibodies for CD68 (AbD Serotec MCA341R, 1:100, AbD Serotec, Oxford, United Kingdom) incubated with horseradish peroxidase-conjugated goat anti-mouse IgG, followed by diaminobenzidine (DAB) for 3 min. The slides were then scanned at 40× magnification using an Aperio ScanScope CS2 slide scanner. Macrophages were quantified as CD68+ cells, using the Positive Pixel Count V9 algorithm within the ImageScope software to detect DAB staining throughout the entire infarct of all 4 tissue sections.

NanoString MULTIPLEX GENE EXPRESSION ANALYSIS. RNA was isolated using the Qiagen RNeasy Fibrous Tissue Mini Kit and the QIAcube Connect nucleic acid isolation robot (QIAGEN, Hilden, Germany) from infarct regions of tissue at 1 week post-injection. For screening of various pathways of interest, RNA samples were analyzed by the NanoString nCounter MAX Analysis System (16,17) with a nCounter custom cardiac codeset (Rat) allowing for multiplexed assessment of 380 genes (see Supplemental Table 1 for full gene list). Samples were processed according to the manufacturer's instructions. In brief, RNA sample concentrations were measured on a Qubit 3.0 Fluorometer (Life Technologies) with a Qubit RNA HS Assay kit. A total of 70 μl of hybridization buffer was mixed with Immunology Panel Reporter CodeSet solution, and 8 μl of this master mix was mixed in a separate reaction vessel with 50 to 100 ng of RNA per tissue sample and RNA-free water up to 13 μl total. A total of 2 μl of Capture ProbeSet was added to each vessel, mixed, and then placed on a thermocycler at 65°C for 16 to 48 h before being maintained at 4°C for <24 h. The NanoString nCounter Prep Station performed automated fluidic sample processing to purify and immobilize hybridized sample to the cartridge surface. Digital barcode reads were analyzed by the NanoString nCounter Digital Analyzer. Results were analyzed by the manufacturer's nSolver Analysis Software version 4.0 and custom R scripts (R Foundation for Statistical Computing, Vienna, Austria). Outliers were detected and excluded based on NanoString's methods for outlier detection.

STATISTICAL ANALYSIS. In vivo functional and histological comparisons between matrix and saline treatment groups were made using a paired *t*-test when comparing baseline to post-injection and Student's *t*-test when comparing matrix-treated to saline control groups. Significance was accepted at $p < 0.05$. Data are reported as mean ± SEM. Gene expression normalization and differential expression were analyzed by the NanoStringDiff package with significance at $p < 0.05$, and adjusted p values were found using the method of Benjamini and Hochberg (18,19). Heatmap was displayed with the pheatmap package (R software Gene enrichment analysis was performed with the clusterprofiler package (20) and Kyoto Encyclopedia of Genes and Genomes (KEGG) pathway images created with the Pathview package (21).

RESULTS

DECELLULARIZED ECM CHARACTERIZATION. The myocardial matrix hydrogel was made using previously described decellularization methods, and standard material characterization analyses were performed for batch quality control (7,10). Here, we also identified the specific protein components that remain post-decellularization using ECM-targeted QconCAT and a liquid chromatography-selected reaction monitoring analysis. Of 83 distinct peptides, which uniquely represent ECM and ECM-associated

FIGURE 1 QconCAT Quantification of Myocardial Matrix Hydrogel

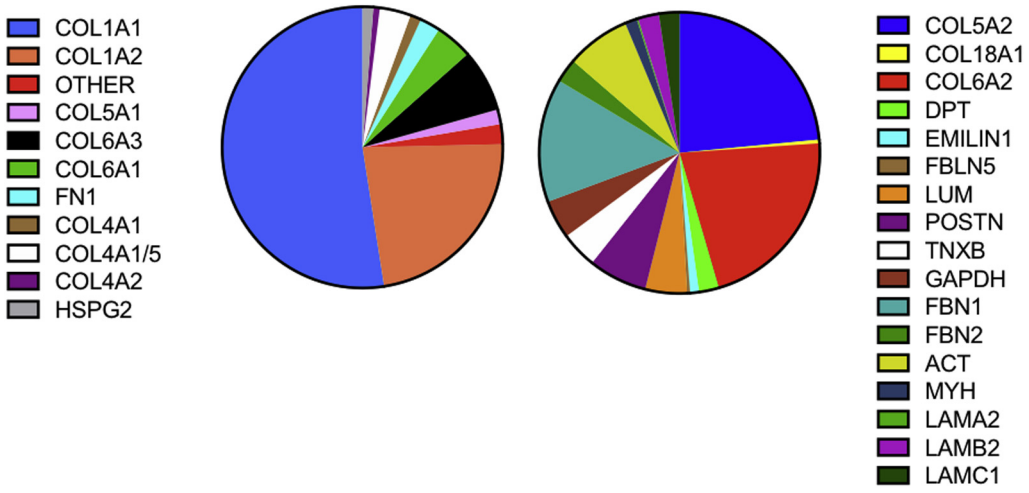

The pie chart shows the average percentage of ECM, ECM-associated, and cellular contaminant protein content as determined using targeted ECM proteomics. ECM = extracellular matrix; QconCAT = quantitative concatamer.

proteins, 28 were detected (**Figure 1 and** Supplemental Table 2). We also performed global proteomics analysis using data-dependent liquid chromatography mass spectrometry (MS)/MS analysis (Supplemental Table 3) because a few ECM proteins, such as collagen 3 alpha-1 chain, are not covered with the QconCAT peptides. The decellularized ECM is composed mostly of fibrillar collagen (types I and III), but also includes numerous other ECM proteins and proteoglycans. The low percentage of cytoskeletal protein contribution (ACT and MYH) indicates the efficiency of the decellularization process (**Figure 1 and** Supplemental Table 2).

EFFECT OF MYOCARDIAL MATRIX HYDROGEL ON NEGATIVE LV REMODELING. We wanted to first evaluate the effects of the myocardial matrix hydrogel on cardiac function in a chronic MI model. Although the scar is generally formed, and there are indications of negative LV remodeling such as fibrosis and LV dilation at 4 weeks post-ischemia reperfusion in rats, we chose an 8-week chronic MI model because previous published reports have shown that cardiac fibrosis, LV dilation, reduced LV peak systolic pressure, increased LV end-diastolic pressure, and cardiac hypertrophy are more pronounced at this time (5,7,22–24). Baseline MR images were taken 1 to 2 days pre-injection (8 weeks post-MI) and 4 weeks post-injection of either matrix (n = 6) or saline (n = 8), as seen in the timeline in **Figure 2**. Representative MR images of saline and matrix injected animals 4 weeks post-injection at end-diastole and end-systole can be seen in **Figures 3A and 3B**, respectively. Comparing matrix-injected animals at baseline versus post-injection, there were no significant changes in LV ESV (131.2 ± 8.3 mm^3 vs. 135.1 ± 13.1 mm^3, n = 6; p = 0.803) and EDV (340.9 ± 19.0 mm^3 vs. 367.9 ± 31.9 mm^3, (n = 6; p = 0.602) (**Figures 3C and 3D**). The saline control group, however, showed significant increases from baseline to post-injection in ESV (148.9 ± 28.2 mm^3 vs. 174.8 ± 25.1 mm^3, n = 8; p = 0.015) and EDV (335.2 ± 21.7 mm^3 vs. 427.9 ± 26.4 mm^3, n = 8; p = 0.011) (**Figures 3C and 3D**). These data are also displayed in Supplemental Table 4. Measurement of changes in myocardial wall thickening in the apical segment indicated that there was significantly reduced LV apical wall thickening in the saline control group (Δ = −0.344 ± 0.122, n = 5) compared with matrix-treated animals (Δ = 0.107 ± 0.080, n = 5; p = 0.015) (**Figure 3E**).

We previously found changes in fibrosis in a subacute MI model (7), and therefore evaluated infarct and interstitial fibrosis at ~5.5 weeks after injection in the chronic MI model (**Figures 4A and 4B**). Analysis shows trends (p = 0.078) for a reduced percentage of fibrosis in the infarct region of matrix-injected hearts (29.53 ± 1.92%, n = 8) compared with the saline control group (35.47 ± 2.50%, n = 6) (**Figure 4C**), although there was no significant difference in myofibroblast density between groups (Supplemental Figure 1). There were no significant differences in

FIGURE 2 **Timeline of Chronic MI Animal Model Showing Long-Term and Short-Term Time Points**

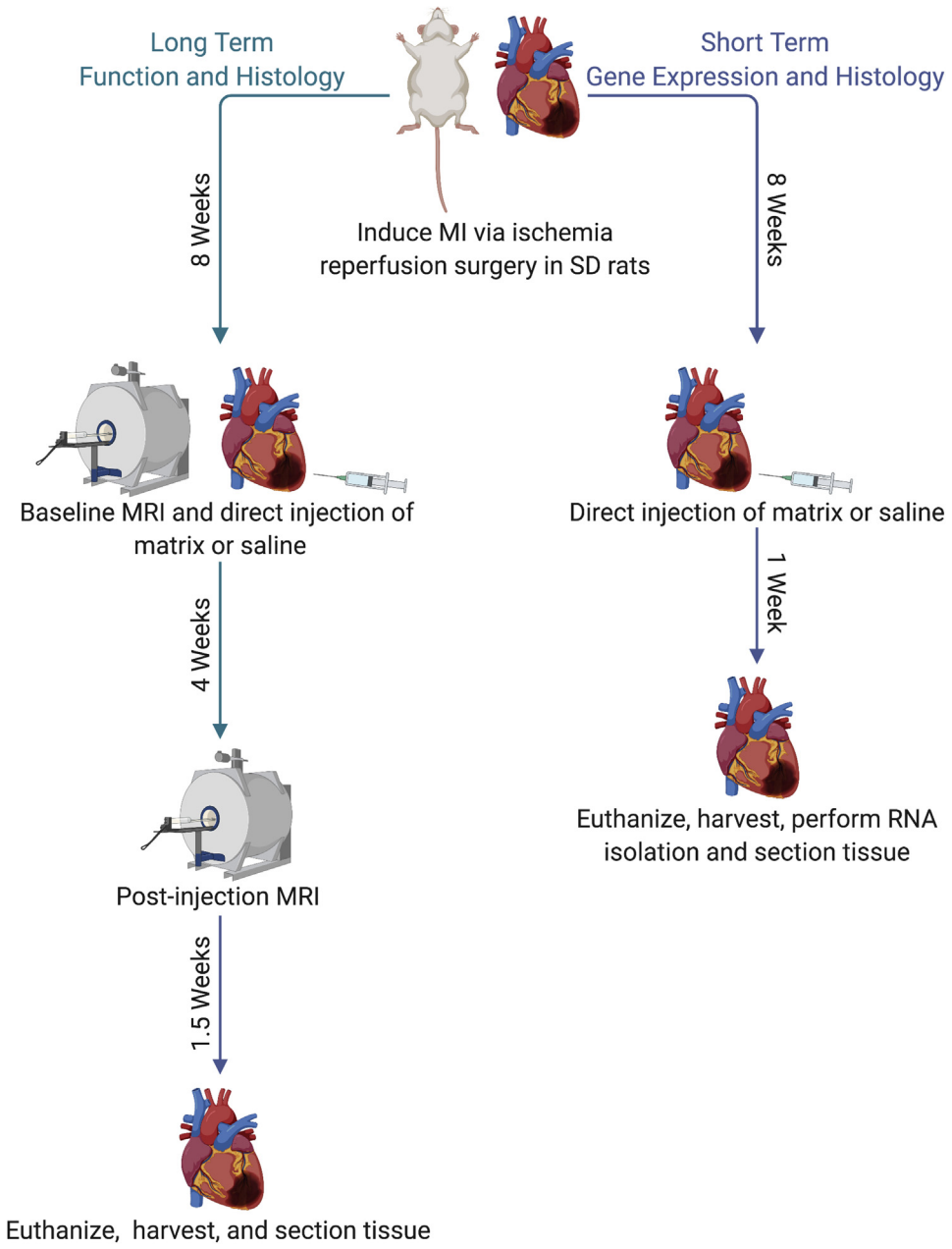

Image created with BioRender (Toronto, Ontario, Canada). MI = myocardial infarction; MRI = magnetic resonance imaging; SD = Sprague Dawley.

percent of interstitial fibrosis in remote myocardium (Supplemental Figure 2) or cardiomyocyte hypertrophy at ~5.5 weeks post-injection (Supplemental Figure 3).

SHORT-TERM GENE EXPRESSION AND HISTOLOGICAL ANALYSES. A custom NanoString nCounter codeset of 380 genes was designed to provide insight into the mechanism of action of the myocardial matrix hydrogel. The panel was designed with the following pathways in mind: fibrosis, immune response (cytokine profile, transcriptional regulation of macrophages and T cells), cardiac muscle contraction and

FIGURE 3 CMR of the Myocardial Matrix Hydrogel

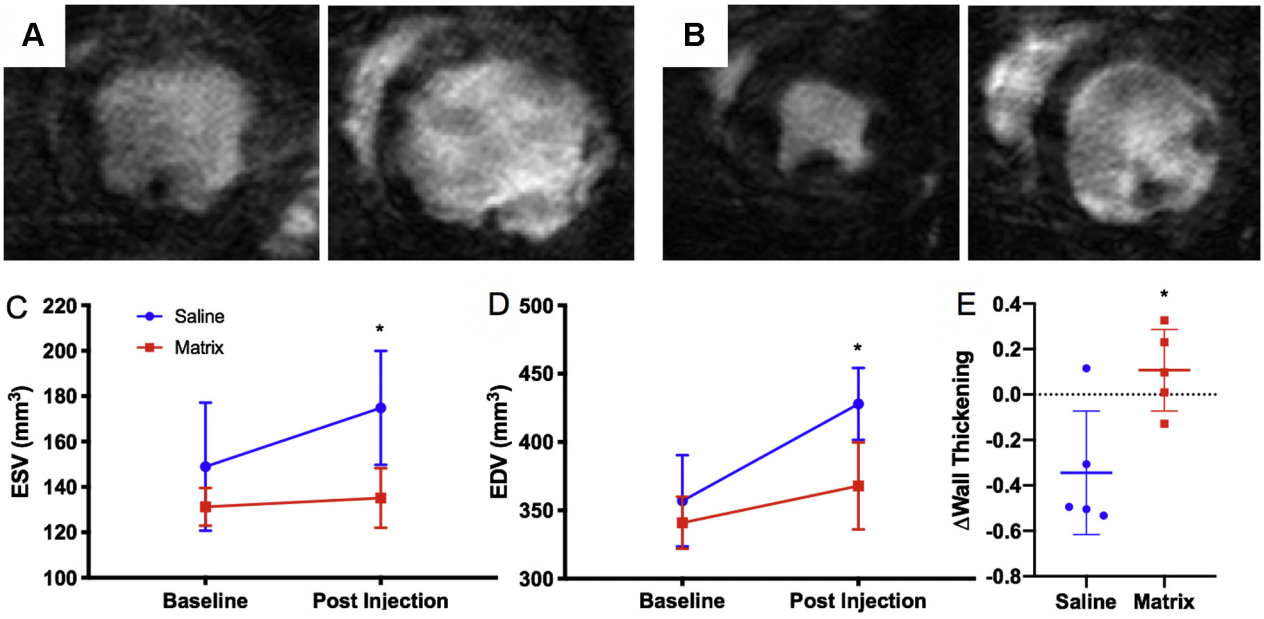

Cardiac magnetic resonance (CMR) imaging shows the myocardial matrix hydrogel preserves LV volumes and improves cardiac wall thickening up to 4 weeks post-injection. Representative MR images of saline control **(A)** and matrix-treated **(B)** animals at 4 weeks post-injection are shown at end systole **(left)** and end diastole **(right)**. MR images were used to determine changes in **(C)** LV ESV and **(D)** LV EDV from baseline (2 days pre-injection, 8 weeks post-MI) and 4 weeks post-injection (12 weeks post-MI). **(E)** Change in wall thickening from baseline to 4 weeks post-injection (Δwall thickening) shows the matrix group was significantly greater than saline controls. *$p < 0.05$ compared with baseline values in **C** and **D**, and compared with saline in **E**. LV = left ventricular; EDV = end-diastolic volume; ESV = end-systolic volume; MI = myocardial infarction.

development, angiogenesis, apoptosis, and cardiac metabolism using published reports to determine key genes from each pathway (8,25-34). The distribution of genes based on these pathways of interest, as well as a full gene list, can be seen in Supplemental Tables 1 and 5. Differential gene expression analyses were performed on isolated infarct tissue samples at 1 week post-injection, as seen in **Figure 2**. Previously, at 1 week post-injection, there were peak cell infiltration into the material and significant shifts in global gene expression in a subacute MI model (8). After 1 week post-injection of either matrix or saline, we saw clustering based on fold change of gene expression of 41 significantly differentially expressed genes (**Figure 5**). Evaluating these differentially expressed genes based on a KEGG pathway enrichment analysis showed hits associated with HF-relevant pathways such as dilated cardiomyopathy, hypertrophic cardiomyopathy, cardiac muscle contraction, adrenergic signaling in cardiomyocytes, and TGF-beta signaling (**Table 1**). Further details, as well as the full list of design pathways and complete list of genes on the nCounter panel, can be found in Supplemental Tables 1 and 5. At 1 week post-injection, there was a significant increase in the expression of ATPase sarcoplasmic/endoplasmic reticulum Ca2+ transporting 1 (Atp2a1), which is crucial for cardiac muscle contraction (**Table 1**). We also saw significant downregulation of transforming growth factor-β (Tgfb3), bone morphogenetic protein-2 (Bmp2), and Bmp4 (**Figure 5**). These genes are involved in the master regulation of fibrogenesis in HF via TGF-β signaling pathways (**Table 1**) (28,35). Additionally, we showed down-regulation of matrix metalloproteinase 2 (Mmp2) and tissue inhibitor of Mmp2 (Timp2), both of which are associated with fibrogenesis in HF (**Figure 5**) (36,37). We also observed down-regulation of Tlr2, Fos, Akt3, Fcer1a, CD68, Cxcl11, and Pf4 and up-regulation of Ccl11, showing modulation of the immune response toward an anti-inflammatory response (**Figure 5**) (32). However, IHC analysis of CD68 staining at 1 week post-injection showed no significant differences in macrophage densities in the infarct region of matrix-injected animals compared with saline (Supplemental Figure 4). Finally, we saw down-regulation of key metabolic genes such as Pdk3 and Akt3, which are involved in glucose oxidation.

FIGURE 4 **Myocardial Matrix Modulates the Fibrotic Response in the Infarct**

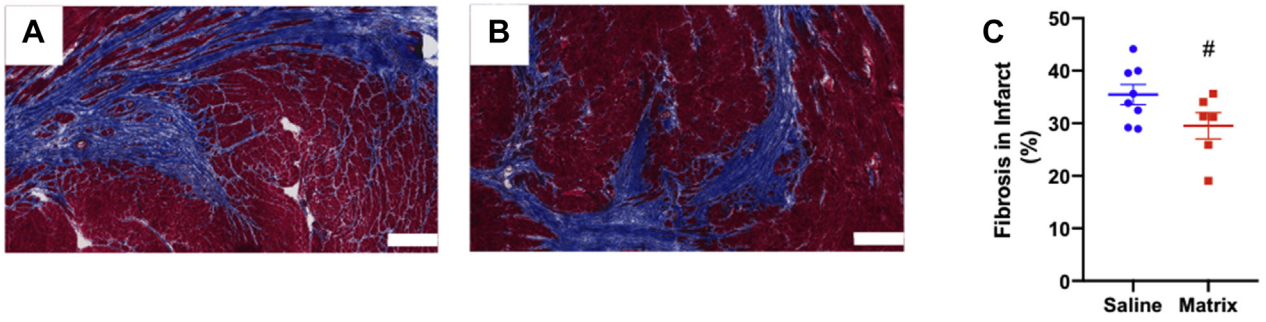

Representative Masson's trichrome staining of saline injected **(A)** and matrix-injected **(B)** infarcts (scale bar = 300 μm) at ~5.5 weeks post-injection. Quantification of infarct fibrosis **(C)**, #p = 0.078.

DISCUSSION

Previous pre-clinical studies have shown efficacy of the myocardial matrix hydrogel in preventing negative LV remodeling and promoting repair in the infarct region in small and large animal subacute MI models (6–8,38). This work led to completion of a phase I clinical trial that showed initial safety and feasibility in human patients, as well as suggested the hydrogel may have potential efficacy in chronic MI (9). This current study, therefore, aimed to show the efficacy and mechanism by which the hydrogel can prevent additional adverse remodeling in a rat model of chronic MI. When the matrix was injected 8 weeks post-MI in the rat model, we observed mitigation of further negative LV remodeling and trends for reduced fibrosis (**Figures 3 and 4**). In vivo gene expression analyses at 1 week post-injection in the chronic MI model showed the importance of differential expression of pathways dysregulated in HF and suppression of chronic inflammation (**Figure 5, Table 1**).

To first confirm efficacy of the matrix in a chronic MI model in vivo, we used CMR to determine changes in cardiac function prior to injection and at 4 weeks post-injection. We demonstrated preserved LV volumes and improved apical wall thickening at 4 weeks post-injection in matrix-injected animals (**Figure 3**), suggesting preservation or improvement in cardiac function. Histological assessments showed a trend for reduced fibrosis in the infarct of matrix-treated animals (**Figure 4**), indicating a possible mechanism of action for preserved cardiac function.

The NanoString custom codeset was designed as a screening tool to be used to provide an initial understanding of what mechanism the matrix may have on a gene expression level in a chronic MI model at 1 week post-injection, a time when there is peak cell infiltration into the scaffold (7). Specifically, we saw up-regulation of key genes involved in the cardiac muscle contraction pathway such as Atp2a1, otherwise known as SERCA1 (**Figure 5**). SERCA1 has previously been shown to improve cardiac muscle contraction in small animal models and other isoforms of SERCA genes have been focused on as a targets for gene therapy in HF (39–41). In subacute MI, it has been shown that the matrix reduces fibrosis up to ~5.5 weeks post-injection; however, the mechanism was not understood (8). In this study, we observed down-regulation of 3 key genes involved in TGF-β signaling (Tgfb3, Bmp2, and Bmp4). TGF-β is a master modulator of fibrogenesis in various diseases, and expression of genes in this pathway are positively correlated with fibrosis (28,35). The matrix may mitigate fibrogenesis through the suppression of TGF-β signaling, specifically Tgfb3, which has been cited as a profibrotic cytokine specific to the chronic MI/HF phase (42).

It has been previously shown that differentiation of fibroblasts toward a myofibroblast phenotype can be important to cardiac repair in the subacute phase of MI; however, long-term persistence and activation can lead to adverse fibrogenesis and negative remodeling associated with HF (43). We did not see any significant differences in myofibroblast density in the infarct of matrix-treated animals compared with the saline control group at ~5.5 weeks post-injection (Supplemental Figure 1). Previous studies have shown that TGF-β signaling is crucial to the fibrogenic activity of myofibroblasts (43,44), and although the

FIGURE 5 Differential Gene Expression Seen at 1 Week Post-Injection of Matrix

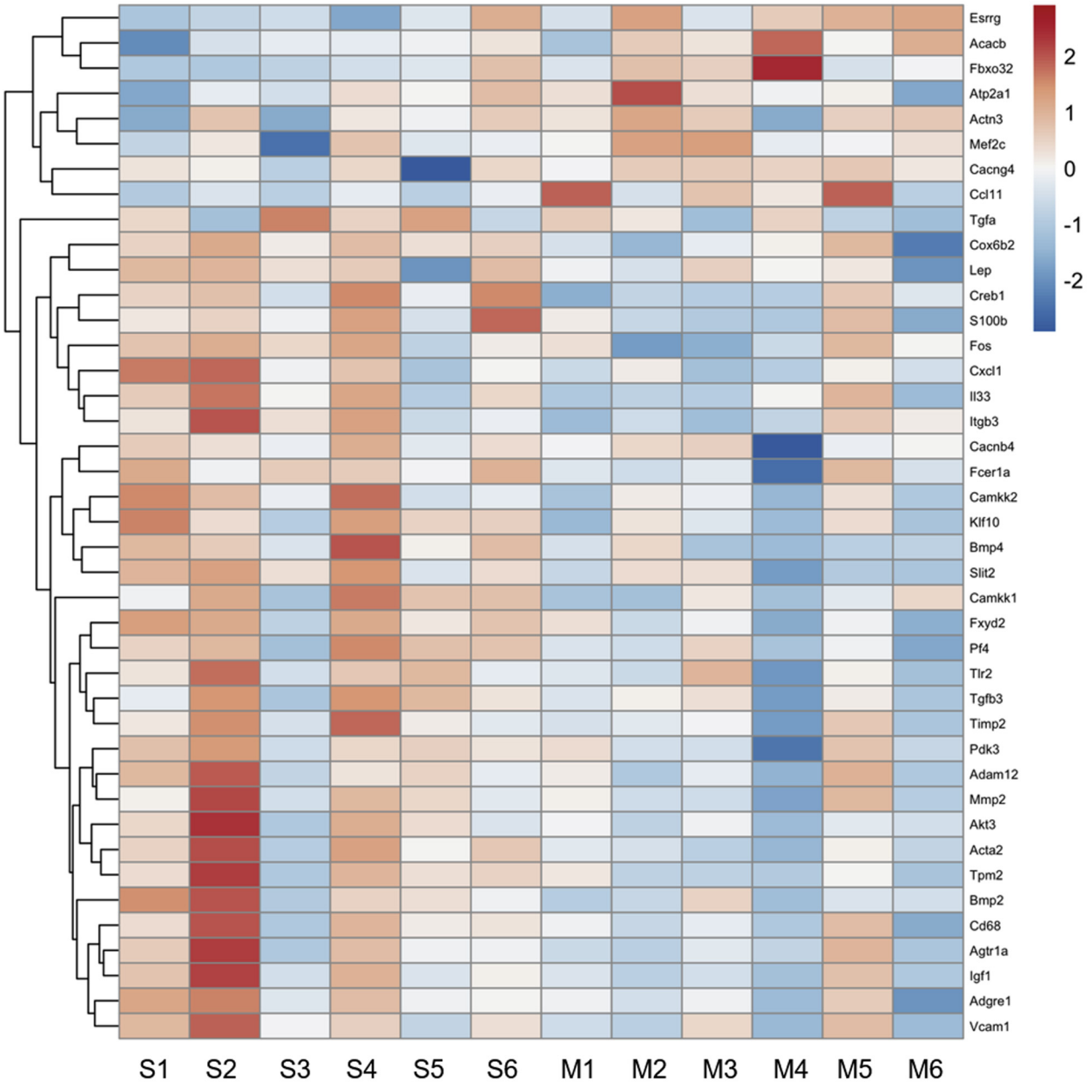

Heatmap of 42 significantly differentially expressed genes show that gene expression in the matrix treatment group (M1-6) is distinct from the saline control group (S1-6) at 1 week post-injection.

matrix was not shown to alter myofibroblast infiltration or density in the infarct, it may still induce a reduction in adverse fibrogenic activity.

Previous studies on the effect of the matrix on cardiac metabolism have shown a rescue of genes involved in oxidative phosphorylation in a subacute model of MI (8). This is beneficial because cardiomyocyte metabolism is notoriously dysregulated in HF with the suppression of oxidative phosphorylation and enhanced dependence on glucose oxidation for ATP supply contributing to energetic inefficiency and adverse remodeling. In this study of

TABLE 1 KEGG Pathway Analysis Results

Pathway ID	Description	Adjusted p Value	geneID
rno05410	Hypertrophic cardiomyopathy	<0.001	Atp2a1/Cacnb4/Cacng4/Igf1/Itgb3/Tgfb3/Tpm2
rno05414	Dilated cardiomyopathy	<0.001	Atp2a1/Cacnb4/Cacng4/Igf1/Itgb3/Tgfb3/Tpm2
rno04261	Adrenergic signaling in cardiomyocytes	<0.001	Agtr1a/Akt3/Atp2a1/Cacnb4/Cacng4/Creb1/Fxyd2/Tpm2
rno04260	Cardiac muscle contraction	<0.001	Atp2a1/Cacnb4/Cacng4/Cox6b2/Fxyd2/Tpm2
rno05418	Fluid shear stress and atherosclerosis	<0.001	Akt3/Bmp4/Fos/Itgb3/Mef2c/Mmp2/Vcam1
rno04060	Cytokine-cytokine receptor interaction	<0.001	Bmp2/Bmp4/Ccl11/Cxcl1/Il33/Lep/Pf4/Tgfb3
rno04152	AMPK signaling pathway	<0.001	Acacb/Akt3/Camkk2/Creb1/Igf1/Lep
rno05412	Arrhythmogenic right ventricular cardiomyopathy	<0.001	Actn3/Atp2a1/Cacnb4/Cacng4/Itgb3
rno04010	MAPK signaling pathway	<0.001	Akt3/Cacnb4/Cacng4/Fos/Igf1/Mef2c/Tgfa/Tgfb3
rno04022	cGMP-PKG signaling pathway	<0.001	Agtr1a/Akt3/Atp2a1/Creb1/Fxyd2/Mef2c
rno04668	TNF signaling pathway	<0.001	Akt3/Creb1/Cxcl1/Fos/Vcam1
rno04657	IL-17 signaling pathway	0.020	Ccl11/Cxcl1/Fos
rno04024	cAMP signaling pathway	0.007	Akt3/Atp2a1/Creb1/Fos/Fxyd2
rno04151	PI3K-Akt signaling pathway	0.009	Akt3/Creb1/Igf1/Itgb3/Tgfa/Tlr2
rno04062	Chemokine signaling pathway	0.018	Akt3/Ccl11/Cxcl1/Pf4
rno04620	Toll-like receptor signaling pathway	0.021	Akt3/Fos/Tlr2
rno04350	TGF-beta signaling pathway	0.021	Bmp2/Bmp4/Tgfb3
rno04922	Glucagon signaling pathway	0.024	Acacb/Akt3/Creb1
rno04960	Aldosterone-regulated sodium reabsorption	0.030	Fxyd2/Igf1
rno04973	Carbohydrate digestion and absorption	0.040	Akt3/Fxyd2

Kyoto Encyclopedia of Genes and Genomes (KEGG) pathway targets and the associated differentially expressed genes at 1 week post-injection.

chronic MI, we did not see up-regulation of genes that regulate oxidative phosphorylation directly, but we found down-regulation of glycolysis/glucose oxidation genes such as Pdk3 and Akt3. These genes are regulators of glucose oxidation, and their long-term up-regulation in HF is linked to negative LV remodeling (45-47). Suppression of these genes suggests the matrix is able to modulate cardiac metabolism in chronic MI.

In subacute MI, there is evidence that the matrix is able to modulate the subacute inflammatory and immune response to promote injury repair, reduce apoptosis of at-risk cardiomyocytes, and promote neovascularization (26,48,49). Interestingly, in this study, we demonstrated an alternate modulation of the inflammatory and immune response. The gene expression analysis shows significant down-regulation of Cd68 and Fcer1a, suggesting reduced migration of immune cells in matrix-treated animals; however, we found no significant histological differences in macrophage density between groups at 1 week post-injection (Supplemental Figure 4). As suggested in previous subacute MI studies of the matrix, the altered gene expression of Cd68 could likely be due to changes in immune cell behavior rather than macrophage infiltration or density (8). Modulation of chronic inflammation may play a role in the mechanism of the matrix in chronic MI because we also saw down-regulation of Mmp2 and Timp2, which are both associated with chronic inflammation in HF leading to fibrosis, increased wall stiffness, and reduced contractility (37). We also found down-regulation of inflammatory cytokines such as Tlr2, Fos, Akt3, Cxcl1, and Pf4. A KEGG pathway enrichment analysis shows Tlr2, Fos, Akt3, Cxcl1, Pf4, Cd68, and Fcer1a are involved in key immune response pathways such as cytokine-cytokine interaction, TNF signaling, toll like receptor signaling, and IL-17 signaling, all of which are known to contribute to adverse remodeling throughout HF (**Table 1**) (26,32,50). This suggests the in vivo reduction in Mmp2/Timp2 may be due to the suppression of inflammation and the proremodeling immune response induced by the matrix. Although acute inflammation and immune response immediately after MI is required to some extent for injury repair, chronic inflammation in HF is associated with the negative feedback loop of continued adverse remodeling (32,50,51).

STUDY LIMITATIONS. This study is limited by the use of a small animal murine model of chronic MI. Although ischemia reperfusion is more representative of the patient population, which is revascularized, the model is not as severe as a permanent ligation model, and therefore, this may have resulted in smaller differences in function and gene expression. Additionally, healing in rats is known to be accelerated, and therefore, the 8-week chronic MI time point is difficult to extrapolate exactly to patients.

However, with the accelerated timing in rats, 8 weeks post-MI is generally accepted as a model for chronic MI in patients due to the extensive scar formation, fibrosis, hypertrophy, and reduced cardiac function consistently seen at this time point in rats. The injection method of direct epicardial injection of the material also does not exactly mimic the transendocardial catheter delivery in human patients; however, catheter delivery requires a large animal, which would make analysis of multiple time points with gene expression and histology difficult. Finally, the nCounter custom codeset was designed for this project with genes across many different pathways for screening for potential mechanisms of action, which limits the analysis in delineating in-depth details of pathway modulation from the material in a chronic MI environment.

CONCLUSIONS

This study is the first investigation to our knowledge into the efficacy and mechanism of a myocardial matrix hydrogel to prevent worsening negative LV remodeling in a small animal model of chronic MI. We observed preserved LV volumes and improved apical wall thickening up to 4 weeks post-injection of the hydrogel, as well as trends for reduced fibrosis. Further, we found the hydrogel modulated key pathways dysregulated in HF such as dilated cardiomyopathy, hypertrophic cardiomyopathy, cardiac muscle contraction, adrenergic signaling in cardiomyocytes, cardiac metabolism, TGF-β signaling, and inflammation.

ACKNOWLEDGMENTS The authors would like to thank Pamela Duran for feedback on the manuscript, and Dr. Elsa Molina of the Sanford Consortium Genomics Core for NanoString analysis preparation and troubleshooting.

FUNDING SUPPORT AND AUTHOR DISCLOSURES

This research was funded in part by the National Institutes of Health National Heart, Lung, and Blood Institute (NHLBI) grant R01HL113468 (Dr. Christman). Ms. Diaz, Dr. Spang, and Dr. Wang were supported by the National Institutes of Health (NIH), NHLBI Training Grant T32HL105373. Ms. Diaz and Dr. Wang were supported by NIH, NHLBI pre-doctoral fellowships F31HL152686 and F31HL137347; and Dr. Spang was supported by an American Heart Association pre-doctoral fellowship. Dr. DeMaria holds equity interest in Ventrix, Inc. Dr. Christman is a cofounder, board member, and consultant for, and holds equity interest in Ventrix, Inc. All other authors have reported that they have no relationships relevant to the contents of this paper disclose.

ADDRESS FOR CORRESPONDENCE: Dr. Karen L. Christman, Department of Bioengineering, University of California, 2880 Torrey Pines Scenic Drive, La Jolla, California 92037, USA. E-mail: christman@eng.ucsd.edu.

PERSPECTIVES

COMPETENCY IN MEDICAL KNOWLEDGE: This study provides the first insight into the mechanism of action of the myocardial matrix injectable hydrogel in chronic MI.

TRANSLATIONAL OUTLOOK: Understanding the mechanism of action of the matrix may guide future clinical studies as well as future design of new therapeutics for HF patients.

REFERENCES

1. Benjamin EJ, Muntner P, Alonso A, et al. Heart disease and stroke statistics-2019 update: a report from the American Heart Association. Circulation 2019;139:e56–528.

2. Diaz MD, Christman KL. Injectable hydrogels to treat myocardial infarction. In: Serpooshan V, Wu S, editors. Cardiovascular Regenerative Medicine. Cham, Switzerland; 2019:185–206.

3. Venugopal JR, Prabhakaran MP, Mukherjee S, Ravichandran R, Dan K, Ramakrishna S. Biomaterial strategies for alleviation of myocardial infarction. J R Soc Interface 2012;9:1–19.

4. Curley CJ, Dolan EB, Otten M, Hinderer S, Duffy GP, Murphy BP. An injectable alginate/extracellular matrix (ECM) hydrogel towards acellular treatment of heart failure. Drug Deliv Transl Res 2019;9:1–13.

5. Landa N, Miller L, Feinberg MS, et al. Effect of injectable alginate implant on cardiac remodeling and function after recent and old infarcts in rat. Circulation 2008;117:1388–96.

6. Singelyn JM, Sundaramurthy P, Johnson TD, et al. Catheter-deliverable hydrogel derived from decellularized ventricular extracellular matrix increases endogenous cardiomyocytes and preserves cardiac function post-myocardial infarction. J Am Coll Cardiol 2012;59:751–63.

7. Seif-Naraghi SB, Singelyn JM, Salvatore MA, et al. Safety and efficacy of an injectable extracellular matrix hydrogel for treating myocardial infarction. Sci Transl Med 2013;5:173ra25.

8. Wassenaar JW, Gaetani R, Garcia JJ, et al. Evidence for mechanisms underlying the functional benefits of a myocardial matrix hydrogel for post-MI treatment. J Am Coll Cardiol 2016;67:1074–86.

9. Traverse JH, Henry TD, Dib N, et al. First-in-man study of a cardiac extracellular matrix hydrogel in early and late myocardial infarction patients. J Am Coll Cardiol Basic Trans Science 2019;4:659–69.

10. Ungerleider JL, Johnson TD, Rao N, Christman KL. Fabrication and characterization of injectable hydrogels derived from decellularized skeletal and cardiac muscle. Methods 2015;84:53–9.

11. Hernandez MJ, Yakutis GE, Zelus EI, et al. Manufacturing considerations for producing and assessing decellularized extracellular matrix hydrogels. Methods 2019;171:20–7.

12. Hill RC, Calle EA, Dzieciatkowska M, Niklason LE, Hansen KC. Quantification of extracellular matrix proteins from a rat lung scaffold to provide a molecular readout for tissue engineering. Mol Cell Proteomics 2015;14:961–73.

13. Singelyn JM, DeQuach JA, Seif-Naraghi SB, Littlefield RB, Schup-Magoffin PJ, Christman KL. Naturally derived myocardial matrix as an

injectable scaffold for cardiac tissue engineering. Biomaterials 2009;30:5409–16.

14. Cerqueira MD, Weissman NJ, Dilsizian V, et al., American Heart Association Writing Group on Myocardial Segmentation and Registration for Cardiac Imaging. Standardized myocardial segmentation and nomenclature for tomographic imaging of the heart. A statement for healthcare professionals from the Cardiac Imaging Committee of the Council on Clinical Cardiology of the American Heart Association. Circulation 2002;105:539–42.

15. Pahlm US, Ubachs JF, Heiberg E, et al. Regional wall function before and after acute myocardial infarction; an experimental study in pigs. BMC Cardiovasc Disord 2014;14:118.

16. Jardine L, Wiscombe S, Reynolds G, et al. Lipopolysaccharide inhalation recruits monocytes and dendritic cell subsets to the alveolar airspace. Nat Commun 2019;10:1999.

17. Hussain S, Johnson CG, Sciurba J, et al. TLR5 participates in the TLR4 receptor complex and promotes MyD88-dependent signaling in environmental lung injury. Elife 2020;9:e50458.

18. Wang H, Horbinski C, Wu H, et al. NanoStringDiff: a novel statistical method for differential expression analysis based on NanoString nCounter data. Nucleic Acids Res 2016;44:e151.

19. Wang H, Zhai T, Wang C. NanoStringDiff: Differential Expression Analysis of NanoString nCounter Data. 2020. R package version 1.20.0. Available at: https://rdrr.io/bioc/NanoStringDiff/. Accessed July 1, 2020.

20. Yu G, Wang L-G, Han Y, He Q-Y. clusterProfiler: an R Package for Comparing Biological Themes Among Gene Clusters. OMICS 2012;16:284–7.

21. Luo W, Brouwer C. Pathview: an R/Bioconductor package for pathway-based data integration and visualization. Bioinformatics 2013;29:1830–1.

22. Omoto ACM, Gava FN, Fazan FS, et al. Myocardial ischemia/reperfusion in rats: characterization of cardiac injuries (abstr). FASEB J 2018;32 Suppl:717–20.

23. Chen Y-F, Weltman NY, Li X, Youmans S, Krause D, Gerdes AM. Improvement of left ventricular remodeling after myocardial infarction with eight weeks L-thyroxine treatment in rats. J Transl Med 2013;11:40.

24. Singal PK, Hill MF. Antioxidant and oxidative stress changes during heart failure subsequent to myocardial infarction in rats. Am J Pathol 1996;148:291–300.

25. Doenst T, Nguyen TD, Abel ED. Cardiac metabolism in heart failure: implications beyond ATP production. Circ Res 2013;113:709–24.

26. Frangogiannis NG. The inflammatory response in myocardial injury, repair, and remodelling. Nat Rev Cardiol 2014;11:255–65.

27. Frangogiannis NG. Pathophysiology of myocardial infarction. Compr Physiol 2015;5:1841–75.

28. Dobaczewski M, Chen W, Frangogiannis NG. Transforming growth factor (TGF)-beta signaling in cardiac remodeling. J Mol Cell Cardiol 2011;51:600–6.

29. Khalil H, Kanisicak O, Prasad V, et al. Fibroblast-specific TGF-beta-Smad2/3 signaling underlies cardiac fibrosis. J Clin Invest 2017;127:3770–83.

30. Noordali H, Loudon BL, Frenneaux MP, Madhani M. Cardiac metabolism - a promising therapeutic target for heart failure. Pharmacol Ther 2018;182:95–114.

31. Nagaraju CK, Robinson EL, Abdesselem M, et al. Myofibroblast phenotype and reversibility of fibrosis in patients with end-stage heart failure. J Am Coll Cardiol 2019;73:2267–82.

32. Riehle C, Bauersachs J. Key inflammatory mechanisms underlying heart failure. Herz 2019;44:96–106.

33. Gaballa MA, Goldman S. Ventricular remodeling in heart failure. J Card Fail 2002;8 Suppl:S476–85.

34. Cahill TJ, Kharbanda RK. Heart failure after myocardial infarction in the era of primary percutaneous coronary intervention: mechanisms, incidence and identification of patients at risk. World J Cardiol 2017;95:407–15.

35. Biernacka A, Dobaczewski M, Frangogiannis NG. TGF-beta signaling in fibrosis. Growth Factors 2011;29:196–202.

36. DeLeon-Pennell KY, Meschiari CA, Jung M, Lindsey ML. Matrix metalloproteinases in myocardial infarction and heart failure. Prog Mol Biol Transl Sci 2017;147:75–100.

37. Kobusiak-Prokopowicz M, Krzysztofik J, Kaaz K, Jolda-Mydlowska B, Mysiak A. MMP-2 and TIMP-2 in patients with heart failure and chronic kidney disease. Open Med (Wars) 2018;13:237–46.

38. Seif-Naraghi SB, Salvatore MA, Schup-Magoffin PJ, Hu DP, Christman K. Design and characterization of an injectable pericardial matrix gel- a potentially autologous scaffold for cardiac tissue engineering. Tissue Eng Part A 2010;16:2017–27.

39. Lalli MJ, Yong J, Prasad V, et al. Sarcoplasmic reticulum Ca2+ ATPase (SERCA) 1a structurally substitutes for SERCA2a in the cardiac sarcoplasmic reticulum and increases cardiac Ca2+ handling capacity. Circ Res 2001;89:160–7.

40. Teucher N, Prestle J, Seidler T, et al. Excessive sarcoplasmic/endoplasmic reticulum Ca2+-ATPase expression causes increased sarcoplasmic reticulum Ca2+ uptake but decreases myocyte shortening. Circulation 2004;110:3553–9.

41. Eisner D, Caldwell J, Trafford A. Sarcoplasmic reticulum Ca-ATPase and heart failure 20 years later. Circ Res 2013;113:958–61.

42. Talman V, Ruskoaho H. Cardiac fibrosis in myocardial infarction-from repair and remodeling to regeneration. Cell Tissue Res 2016;365:563–81.

43. Turner NA, Porter KE. Function and fate of myofibroblasts after myocardial infarction. Fibrogenesis Tissue Repair 2013;6:5.

44. Yousefi F, Shabaninejad Z, Vakili S, et al. TGF-β and WNT signaling pathways in cardiac fibrosis: non-coding RNAs come into focus. Cell Commun Signal 2020;18:87.

45. Wende AR, O'Neill BT, Bugger H, et al. Enhanced cardiac Akt/protein kinase B signaling contributes to pathological cardiac hypertrophy in part by impairing mitochondrial function via transcriptional repression of mitochondrion-targeted nuclear genes. Mol Cell Biol 2015;35:831–46.

46. Taniyama Y, Ito M, Sato K, et al. Akt3 overexpression in the heart results in progression from adaptive to maladaptive hypertrophy. J Mol Cell Cardiol 2005;38:375–85.

47. Gray LR, Tompkins SC, Taylor EB. Regulation of pyruvate metabolism and human disease. Cell Mol Life Sci 2014;71:2577–604.

48. Somasundaram P, Ren G, Nagar H, et al. Mast cell tryptase may modulate endothelial cell phenotype in healing myocardial infarcts. J Pathol 2008;205:102–11.

49. Bischoff SC. Role of mast cells in allergic and non-allergic immune responses: comparison of human and murine data. Nat Rev Immunol 2007;7:93–104.

50. Ong SB, Hernandez-Resendiz S, Crespo-Avilan GE, et al. Inflammation following acute myocardial infarction: multiple players, dynamic roles, and novel therapeutic opportunities. Pharmacol Ther 2018;186:73–87.

51. Aurora AB, Porrello ER, Tan W, et al. Macrophages are required for neonatal heart regeneration. J Clin Invest 2014;124:1382–92.

KEY WORDS biomaterials, chronic inflammation, chronic myocardial infarction, gene expression

APPENDIX For supplemental figures and tables, please see the online version of this paper.